ChemistryOpen

Research Article
doi.org/10.1002/open.202200116

Chemistry Europe
European Chemical Societies Publishing

www.chemistryopen.org

Special Collection

Characterization of Diastereomeric Equilibria of Pseudotetrahedral Bis[(*R* or *S*)-*N*-1-(Ar)Ethylsalicylaldiminato-κ²N,O]zinc(II) with Λ/Δ-Chirality-At-Metal Induction

Mohammed Enamullah,*[a] Mohammad Mostafizur Rahman,[a] Mohammad Khairul Islam,[a] Dennis Woschko,[b] Christoph Janiak,*[b] and Gennaro Pescitelli*[c]

A family of bis[(*R* or *S*)-*N*-1-(Ar)ethylsalicylaldiminato-κ²N,O]-Δ/Λ-zinc(II) {Ar=C_6H_5 (Zn*R*L[1] or Zn*S*L[1]), *p*-$CH_3OC_6H_4$ (Zn*R*L[2] or Zn*S*L[2]) and *p*-ClC_6H_4 (Zn*R*L[3] or Zn*S*L[3])} compounds was synthesized and investigated by multiple methods. They feature Λ/Δ-chirality-at-metal induction along the pseudo-C_2 axis of the molecules. The chirality induction is quantitative in the solid state, explored by X-ray crystallography and powder X-ray diffraction (PXRD), where *R* or *S*-ligated complexes diastereoselectively yield Λ or Δ-configuration at the metal. On the other hand, Λ and Δ-diastereomers co-exist in solution. The Λ⇆Δ equilibrium is solvent- and temperature-dependent. Electronic circular dichroism (ECD) spectra confirm the existence of a diastereomeric excess of Λ-Zn*R*L[1–3] or Δ-Zn*S*L[1–3] in solution. DSC analysis reveals thermally induced irreversible phase transformation from a crystalline solid to an isotropic liquid phase. ECD spectra were reproduced by DFT geometry optimizations and time-dependent DFT (TD-DFT) calculations, providing ultimate proof of the dominant chirality atmetal in solution.

Introduction

Transition metal complexes with chiral Schiff base ligands are of continued interest[1–12] and developed for applications as chiral catalysts for the synthesis of organic and inorganic compounds.[13–14] We have recently reported on the synthesis, characterization, chiroptical properties, supramolecular chemistry, (dia)stereoselectivity and X-ray molecular structures along with computational studies of four-coordinated chiral [M(*R* or *S*-NO)$_2$] complexes (NO = deprotonated Schiff bases, M=Co/Cu/Ni/Zn) with Λ/Δ-chirality-at-metal induction in tetrahedral or distorted tetrahedral/square-planar geometry.[15–26] Coordination of the enantiopure ligands (*R* or *S*-NO) to the metal leads to the formation of two diastereomers Λ-M-*R*-NO and Δ-M-*R*-NO (or Λ-M-*S*-NO and Δ-M-*S*-NO), while the racemic ligands (*R*/*S*-NO) give all four diastereomers. The non-covalent interactions acting within the metal-chiral ligands framework in the solid state, or solute-solvent interactions in solution, provide a difference in free energy between the two diastereomers and, hence, result in one thermodynamically favored diastereomer.[15,27–28] The Λ/Δ-chirality-at-metal induction arises exclusively (i.e., Λ-*R* or Λ-*S* as the only diastereomer) in an enantiopure crystal in the solid state, as evidenced by X-ray structure determination. However, it must be stressed that the measurement of a single crystal does not exclude the presence of other minor diastereomers in bulk solid-state samples. An alternative method, differential scanning calorimetry (DSC) for solid-state samples, provides both quantitative and qualitative information on Δ- and/or Λ-diastereomers based on thermally induced phase transformations from a crystalline solid to an isotropic liquid phase.[21] Moreover, in solution, both Λ- and Δ-diastereomers coexist with an uneven ratio and show a temperature-dependent dynamic diastereomeric equilibrium (Λ⇆Δ), evidenced by NMR, electronic circular dichroism (ECD) and vibrational circular dichroism (VCD) studies.[17,21] ECD/VCD spectra reveal expected mirror image relationships for complexes obtained from enantiomeric ligands in solution. In addition, these spectra are dominated by the chirality atmetal. Thus, comparing experimental ECD/VCD spectra with calculations allows for the assignment of the preferential chirality atmetal. Moreover, ECD/VCD spectra may be employed to study the diastereomeric equilibrium in solution.

Our recent studies on diastereoselection phenomena of metal(II) complexes (metal = Co/Cu/Ni/Zn) with enantiopure (Ar)salicylaldiminate/naphthaldiminate ligands revealed that

[a] Prof. Dr. M. Enamullah, M. Mostafizur Rahman, M. Khairul Islam
Department of Chemistry
Jahangirnagar University
1342 Dhaka (Bangladesh)
E-mail: enamullah@juniv.edu
[b] Dr. D. Woschko, Prof. Dr. C. Janiak
Institute of Inorganic Chemistry and Structural Chemistry
Heinrich-Heine-University of Düsseldorf
40204 Düsseldorf (Germany)
E-mail: janiak@uni-duesseldorf.de
[c] Prof. Dr. G. Pescitelli
Department of Chemistry and Industrial Chemistry
University of Pisa
56124 Pisa (Italy)
E-mail: gennaro.pescitelli@unipi.it

Supporting information for this article is available on the WWW under https://doi.org/10.1002/open.202200116

An invited contribution to a Special Collection dedicated to the latest research of ChemistryOpen's Editorial Advisory Board Members.

the Λ/Δ-chirality-at-metal induction is typically controlled by the chirality of the *R* or *S*-ligand, in general providing the Λ-M*R* or Δ-M*S* diastereomer in the solid state and a diastereomeric excess of Λ-M*R* or Δ-M*S* in solution.[17,18,20–22,25,26] ^{1}H NMR spectra for diamagnetic Zn complexes[17,21] clearly display both Δ- and Λ-diastereomers with an uneven ratio for each enantiopure complex, and also show an equilibrium shift (Δ⇆Λ) depending on both time and temperature in solution. Different substitution patterns at the salicylic phenyl ring, such as the introduction of two halogen substituents, did not alter the preference for Λ-Zn*R* or Δ-Zn*S* diastereomers both in solution and in the solid state.[26] This is opposite to what has been observed for homoleptic Cu complexes, where the presence of di-halogen substituents resulted in a chirality-at-metal inversion from Λ-Cu*R* or Δ-Cu*S* (in solid state) to Δ-Cu*R* or Λ-Cu*S* (in solution).[23] Surprisingly, ^{1}H NMR studies indicate the formation of only one diastereomer (Λ-Zn*R* or Δ-Zn*S*) in the bulk samples of the former homoleptic Zn complexes with di-halogen substituents[26] (also supported by the simulated spectra), contrary to analogous Zn complexes without substituents.[17,21] The phenomenon is further influenced by solvent polarity, pH of the solution, metal ion selection, redox state and crystallization protocol.[29–30]

We herein report the synthesis, spectroscopy, thermal analyses, powder X-ray diffraction (PXRD) and X-ray structure of a family of *bis*[{(*R* or *S*)-N-(Ar)ethylsalicylaldiminate-κ^{2}N,O}]-Λ/Δ-zinc(II) complexes with Ar=C_6H_5 (ZnL^1), *p*-$CH_3OC_6H_4$ (ZnL^2) and *p*-ClC_6H_4 (ZnL^3). The X-ray structure for compound ZnL^1 was reported before.[5c–d] The difference with our X-ray structure for Zn*R*L^1 is noticed in the Supporting Information. Also, the ECD spectrum of ZnL^1 has been measured previously,[5c,31] but density functional theory (DFT) calculations of geometries and ECD spectra had not been reported. Compounds ZnL^2 and ZnL^3 have also previously been reported on and had been examined by X-ray and VCD analyses.[17] Preliminary ECD spectra were also reported,[17] which will be recalled later. The present study mainly focuses on ^{1}H NMR/ECD spectra at variable temperature/time and in different solvents to analyze, in detail, the impact of various variables on the phenomena of diastereoselection and chirality-at-metal induction. A thorough computational study was employed to get insight into chiroptical properties and to interpret the preferred formation of diastereomer (Λ vs. Δ) through comparisons of experimental and calculated ECD spectra. In this way, we complete our survey on the homoleptic series of ligands L^1-L^3 in several metal complexes,[17,19,20a,22] and provide new comparison to the behavior of the analogous Zn^{II}-(Ar)naphthaldiminate series.[21]

Results and Discussion

Synthesis

The enantiopure Schiff base ligands (*R* or *S*)-*N*-1-(Ar)ethylsalicylaldimine (HL$^{1-3}$)[15] react with zinc(II) acetate, under reflux, to give the enantiopure bis[(*R* or *S*)-*N*-1-(Ar)ethylsalicylaldiminato-κ^{2}N,O]zinc(II) {Ar=C_6H_5 (Zn*R*L^1 or Zn*S*L^1), *p*-$CH_3OC_6H_4$ (Zn*R*L^2 or Zn*S*L^2) and *p*-ClC_6H_4 (Zn*R*L^3 or Zn*S*L^3)} compounds, respectively, with Λ/Δ-chirality-at-metal induction (Scheme 1). IR spectra show strong bands at 1600–1625 cm^{-1} ($\nu_{C=N}$) for the imine group in the complexes. EI-mass spectra show the parent ion peaks at *m/z*=512 (Zn*R*L^1 or Zn*S*L^1), 572 (Zn*R*L^2 or Zn*S*L^2) and 582 (Zn*R*L^3 or Zn*S*L^3) in addition to several ions peaks for the fragmented species including $[M-L]^+$, $[HL]^+$, $[C_6H_4(O)(CHNH)Zn]^+$, $[C_6H_4(OCH_3)(CHNH)]^+$ and $[C_6H_4(Cl)(CHNH)]^+$ (see Supporting Information for spectral data).

Solid-State Structure

Single-crystal X-ray structure analyses for bis[(*R* or *S*)-*N*-1-(Ar)ethylsalicylaldiminato-κ^{2}N,O]zinc(II) {Ar=C_6H_5 (Zn*R*L^1 or Zn*S*L^1), *p*-$CH_3OC_6H_4$ (Zn*R*L^2 or Zn*S*L^2) and *p*-ClC_6H_4 (Zn*R*L^3 or Zn*S*L^3)} show that the two NO-chelate Schiff bases form a pseudotetrahedral N_2O_2-coordination sphere around the zinc atom with Λ/Δ-chirality induction along the pseudo-C_2 axis of the molecules (Figure 1). The *R* or *S*-ligand chirality diastereoselectively gives Λ-Zn*R*L$^{1-3}$- or Δ-Zn*S*L$^{1-3}$-configured complexes in an enantiopure single crystal.[5,17,21] The structures for Λ-Zn*R*L^1 [5c] or Δ-Zn*S*L^1 [5d] (Ar=C_6H_5) show two symmetry-independent molecules (Zn1/Zn2, Figure S1, Supporting Information) with identical configuration atmetal in the asymmetric unit to give *Z*′=2 structures, which we confirmed through a structure re-determination for Zn*R*L^1 (see Supporting Information for details). On the other hand, the analogous Zn*R*L$^{2-3}$ or Zn*S*L$^{2-3}$ species with *p*-methoxy/-chloro-substituents on the phenyl group (Ar=*p*-$CH_3OC_6H_4$ and *p*-ClC_6H_4) only provide a single molecule in the asymmetric unit.[17] For Λ-Zn*R*L$^{1-3}$ or Δ-Zn*S*L$^{1-3}$,

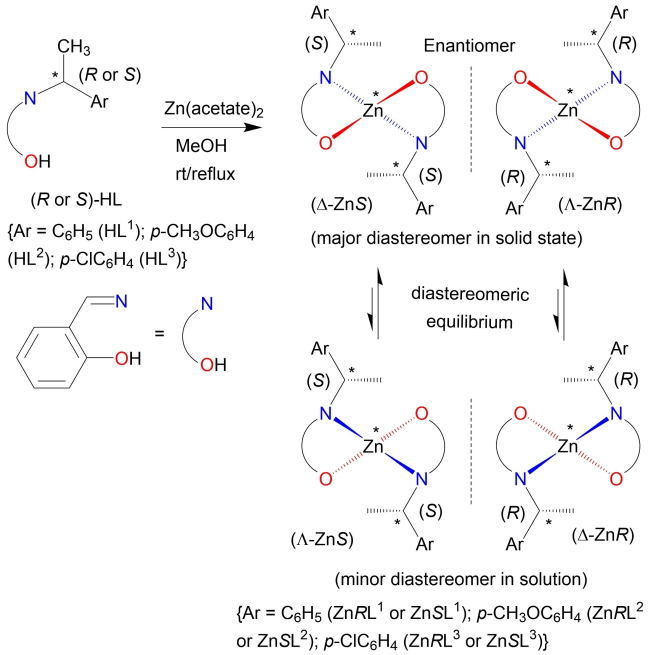

Scheme 1. Synthetic route to bis[(*R*- or *S*)-*N*-1-(Ar)ethylsalicylaldiminato-κ^{2}N,O]-Λ/Δ-zinc(II) compounds.

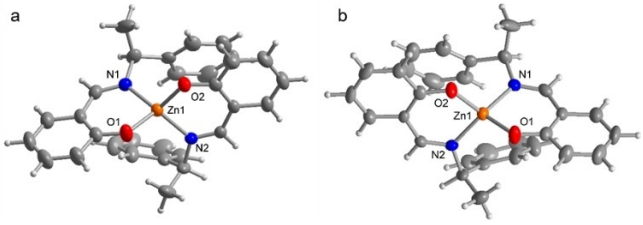

Figure 1. Molecular structures of (a) Δ-Zn*S*L[1] and (b) Λ-Zn*R*L[1] (depicting only one of the two symmetry-independent molecules in each case) to present the pseudotetrahedral geometries with approximate C_2-symmetry in the structures of Zn*R*L[1–3] or Zn*S*L[1–3] (50% thermal ellipsoids). The structure shown in (b) is a re-determination (see Supporting Information for details); in (a), the structure was re-drawn from the deposited CIF file of CCDC 856921.[5d]

the two coordinated ligands are crystallographically independent; the zinc atoms sit on a general position. Still, the complexes exhibit an approximately C_2-symmetric arrangement (cf. Scheme 1) with the assumed C_2-axis dissecting the O–Zn–O and the N–Zn–N angles. Selected bond lengths and angles for Λ-Zn*R*L[1] or Δ-Zn*S*L[1] are listed in Table S1 (Supporting Information), comparable to the analogous Zn^{II}-(*S*)-(phenyl)ethylsalicylaldiminates.[5d]

The structures of the analogous M^{II}-(*R* or *S*)-(Ar)naphthaldiminates (M=Zn[17] and Ni[20]) also contained two symmetry-independent molecules in the asymmetric unit with the same metal configuration (i.e., Λ-M*R*L or Δ-M*S*L diastereomer), while the Cu^{II}-(*R*)-(Ar)naphthaldiminates (Ar = *m*-$CH_3OC_6H_4$)[18] show two symmetry-independent molecules in the asymmetric unit with opposite configuration atmetal (i.e., Λ/Δ-Cu*R*L, diastereomeric pair). However, a consistent stereochemical chirality-at-metal induction is reported for the analogous M^{II}-(*R* or *S*)-(Ar) salicylaldiminates/naphthaldiminates (M=Co,[22,25] Ni,[20] Cu,[18,23] and Zn[5c–d,17,21,26]) to provide Λ-M*R*L or Δ-M*S*L diastereomers for *R* or *S*-HL ligands. Only in a single case, opposite chirality-at-metal induction has been reported to give Δ-Cu*R*L or Λ-Cu*S*L in the case of Cu^{II}-(*R* or *S*)-(Ar)salicylaldiminates.[19]

Powder XRD Analyses

PXRD patterns for the enantiopure complexes (Zn*R*L[1–3]/Zn*S*L[1–3]) were measured at 2θ = 5–50° and ambient temperature, and they feature consistent similarities along the series (Figures 2 and S2). The experimental PXRD patterns fit well with the simulated patterns from the single-crystal structures,[5d,17] confirming the phase purity of the bulk samples of the complexes.[23,26]

Thermal Analyses

Thermally induced structural phase transformation from distorted tetrahedral/square-planar in solid-state (at low temperature) to regular tetrahedral/square-planar geometry in the isotropic liquid phase (at high temperature) is well known for transition metal-Schiff base complexes,[18,20–23,25] furthermore offering an indication of the thermal stability of the complexes. The differential scanning calorimetry (DSC) heating curves display a strong endothermic peak with large heat absorption or transformation at 175–176 °C for Zn*R*L[1]/Zn*S*L[1], 186–187 °C for Zn*R*L[2]/Zn*S*L[2] and 165–169 °C for Zn*R*L[3]/Zn*S*L[3] (Figure 3 and S3 and Table 1), while cooling curves show no peak on the reverse direction. DSC results thus suggest a thermally induced irreversible phase transformation from the crystalline solid to the isotropic liquid phase.[18,20–23,25] The presence of a single endothermic peak corresponds to a single diastereomer Λ-Zn*R*L[1–3] or Δ-Zn*S*L[1–3] in the bulk sample in the solid state, in parallel to the X-ray structures for the complexes. Similar results with only a single DSC peak were found for each enantiopure complex of analogous M^{II}-(Ar)salicylaldiminates/naphthaldiminates (M=Co,[22,25] Cu,[18,23] Ni[20]), while two separate peaks corresponding to both Λ- and Δ-diastereomers with an uneven

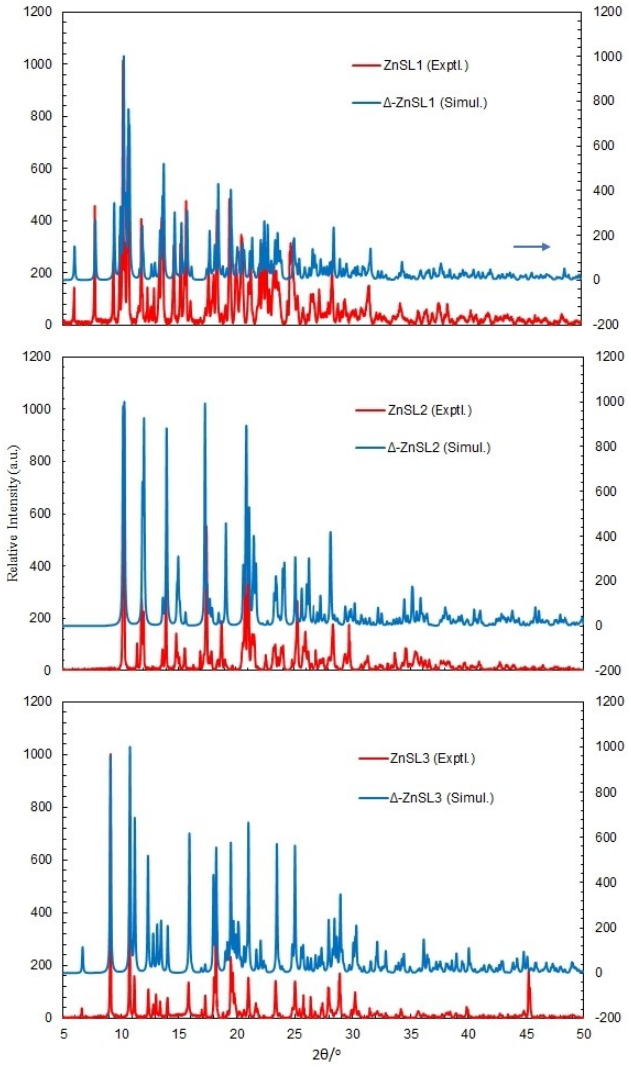

Figure 2. Experimental and simulated PXRD patterns for Zn*S*L[1–3] at ambient temperature. The simulated patterns are based on the deposited CIF files with CCDC numbers 856921, 841950 and 841952 for Δ-Zn*S*L[1–3], respectively.

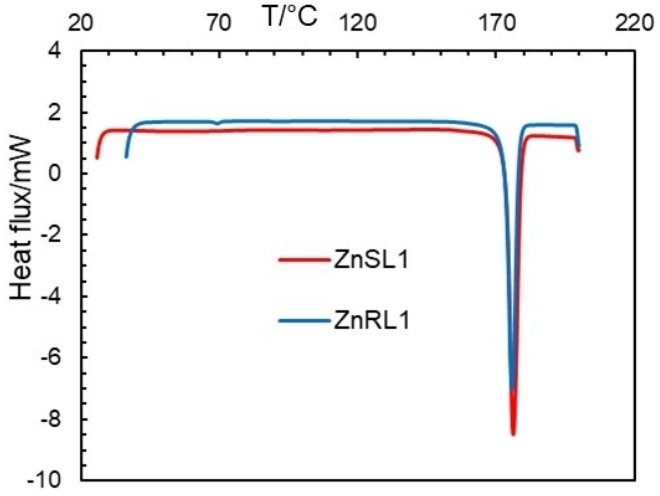

Figure 3. Differential scanning calorimetry (DSC) heating curves for Zn*R*L[1] and Zn*S*L[1] complexes.

Table 1. DSC data for Zn*R*L[1–3] or Zn*S*L[1–3] complexes.[a,b]

Compound	Heating curve Peak temp. [°C]/ΔH[c]
Zn*R*L[1]	175.1/−25.14
Zn*S*L[1]	176.2/−30.13
Zn*R*L[2]	186.5/−46.53
Zn*S*L[2]	185.7/−42.02
Zn*R*L[3]	165.4/−19.21
Zn*S*L[3]	169.3/−27.94

[a] DSC analyses were run just before the decomposition temperature of the complexes. [b] All data shown for the first run. No peak on cooling curve was observed for each sample. [c] ΔH = heat of transformation in kJ mol^{-1}

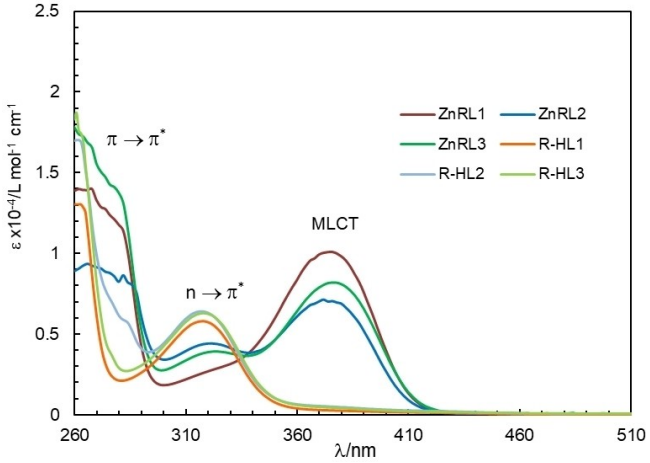

Figure 4. Absorption spectra for free Schiff base ligands (*R*-HL[1–3]) and corresponding Λ-Zn*R*L[1–3] complexes (0.7–1.6 mM) in chloroform at 25 °C.

Table 2. Absorption data for the free Schiff base ligands (0.2–0.3 mM) and their Zn complexes (0.8–1.6 mM) in chloroform at 25 °C.

Compound	Transition λ_{max} (ε_{max})[a] π→π*	n→π*	MLCT
Λ-Zn*R*L[1]	≈280 sh	324 (1680)	376 (5925)
R-HL[1]	nd	318 (5811)	nd
Δ-Zn*S*L[1]	≈280 sh	324 (3511)	374 (6928)
Λ-Zn*R*L[2]	≈280 sh	322 (4351)	372 (7023)
R-HL[2]	nd	317 (6409)	nd
Δ-Zn*S*L[2]	≈280 sh	320 (5398)	374 (5894)
Λ-Zn*R*L[3]	≈280 sh	324 (3811)	376 (7933)
R-HL[3]	nd	318 (6287)	nd
Δ-Zn*S*L[3]	≈280 sh	324 (1950) sh	378 (6788)

[a] λ in nm and ε in L mol^{-1} cm^{-1}; sh = shoulder; nd = not detected.

ratio were reported for each enantiopure complex of Zn^{II}-(Ar)naphthaldiminates.[21]

Absorption Spectra

Absorption spectra for enantiopure Schiff base ligands and enantiopure Zn^{II}-Schiff base complexes in chloroform show consistent similarities along the series (Figures 4 and S4, and Table 2). The spectral patterns for the Schiff base ligands are quite different from those of the complexes. The spectra feature a strong band below 300 nm and a moderately intense band at 300–350 nm with maxima at λ_{max} = 320–325 nm, due to the intra-ligand π→π* and n→π* transitions, respectively.[17,21,26] The spectra for the complexes further show a strong broad band at 350–420 nm with λ_{max} = 372–378 nm, assigned to the metal-ligand charge transfer (MLCT) transitions, which are obviously absent in the Schiff base ligands. Absorption spectra recorded at different time intervals suggest a rapid decomposition of the complex upon dissolution in chloroform (Figure 5): the intra-ligand n→π* band becomes more intense, while the MLCT band completely disappears over time. Almost 90% decomposition is observed within one hour, and full

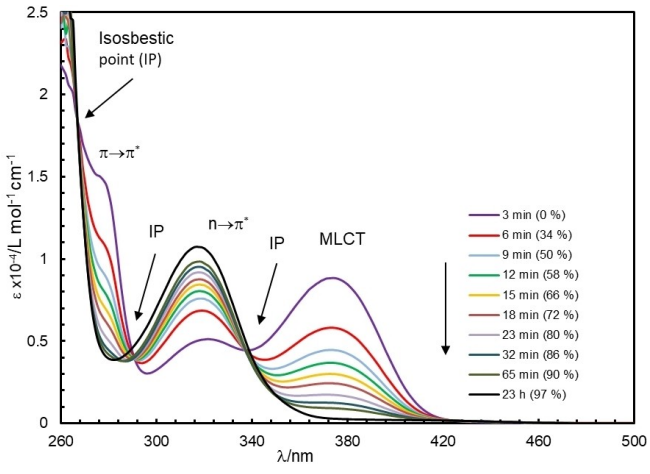

Figure 5. Absorption spectra of bis[(*S*)-*N*-1-(C_6H_5)ethylsalicylaldiminato-κ^{2}N,O]-Δ-zinc(II), (Zn*S*L[1]) at different time intervals in chloroform at 25 °C.

decomposition with fading of the orange-yellow color in one day. The rapid decomposition might be due to the presence of a small amount of water and/or acidity in chloroform which leads to hydrolysis of the complexes. Indeed, the presence of three isosbestic points at 267, 290 and 340 nm corresponds to

the existence of an equilibrium between the complexes and the free ligands. The same experiment in a non-polar solvent like cyclohexane suggests a somewhat slower decomposition, reaching ca. 20% within one hour and ca. 95% in 18 h (Figure S5). These results are in line with the common feature for four-coordinated labile pseudo-tetrahedral Zn^{II}-Schiff bases complexes in solution.[17,21,26]

Electronic Circular Dichroism (ECD) Spectra

Electronic circular dichroism (ECD) spectra of complexes prepared from enantiomeric ligands, for example, Zn*R*L^1 vs. Zn*S*L^1, Zn*R*L^2 vs. Zn*S*L^2, and Zn*R*L^3 vs. Zn*S*L^3, show the expected mirror image relationships, thus confirming the diastereomeric purity or diastereomeric excess of the complexes in chloroform (Figure 6 and Table 3). The spectra for the complexes derived from *R* ligands show a negative couplet with extrema at λ_{max} = 352–355 and 387–389 nm, a small negative band with its minimum at 319–322 nm, and a positive band below 300 nm (which is poorly defined due to the solvent cutoff). The reverse signs are observed for the complexes obtained from *S* ligands. The bands at λ_{max} = 282–287 and 319–322 nm are associated to the intra-ligand $\pi\rightarrow\pi^*$ and $n\rightarrow\pi^*$ transitions, respectively, while the bands at λ_{max} = 352–355 and 387–389 nm are due to the MLCT transitions. The spectra are consistent with those reported before,[5c,17,31] though of overall better quality for ZnL^{2,3} for which the mirror-image appearance between enantiomeric species was not fully reflected in a previous publication.[17] A theoretical analysis of ECD spectra is reported in a separate section below.

^{1}H NMR Spectral Analyses

^{1}H NMR spectra for the Zn*R*L^1 and Zn*S*L^2 complexes are displayed in Figure 7. The methyl protons appear as a doublet at δ 1.45–1.51 ppm (J = 6.6 Hz) and the methine proton appears as a quartet at δ 4.21–4.28 ppm (J = 6.6 Hz). The imine proton appears as a singlet at δ 7.95–8.03 ppm, which is shifted upfield by 0.25–0.45 ppm in comparison to the free Schiff bases (δ 8.20–8.45 ppm),[15] indicating coordination of the nitrogen atom to the Zn^{2+} ion. Further, the methoxy protons appear as a singlet at δ 3.75 ppm in Zn*R*L^2 or Zn*S*L^2. Several aromatic proton peaks appear as doublet, triplet and multiplet in the range of δ 6.60–7.50 ppm, respectively (Figure 7 and Supporting Information). The phenolic proton peak, usually observed as a broad signal at δ 14.72–14.85 ppm in the free Schiff bases due to strong intermolecular hydrogen bonding,[15] is absent in the complexes, confirming the formation of an ionic bond between Zn^{2+} and O^- ions. A small residual peak (asterisked in Figure 7)

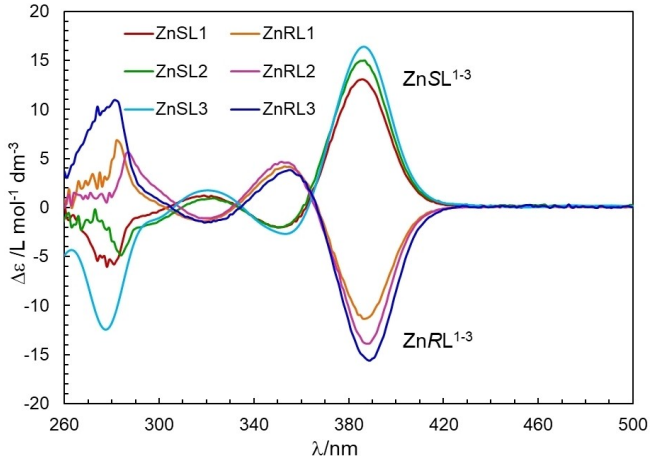

Figure 6. Electronic circular dichroism (ECD) spectra for bis[(*R* or *S*)-*N*-1-(Ar)ethylsalicylaldiminato-κ^{2}N,O]-Δ/Λ-zinc(II) (1.4–2.6 mM) in chloroform at 25 °C (cell path length 0.1 cm).

Table 3. ECD spectral data for bis{(*R* or *S*)-*N*-1-(Ar)ethylsalicylaldiminato-κ^{2}N,O}-Δ/Λ-zinc(II) (1.4–2.6 mM) in chloroform at 25 °C.

Compound	Transition λ_{max} (ε_{max})[a] $\pi\rightarrow\pi^*$	$n\rightarrow\pi^*$	MLCT	MLCT
Λ-Zn*R*L^1	≈280 (+)[b]	319 (−1.4)	353 (+4.2)	387 (−11.4)
Δ-Zn*S*L^1	≈280 (−)[b]	319 (+1.3)	350 (−2.1)	386 (+13.0)
Λ-Zn*R*L^2	≈280 (+)[b]	321 (−1.0)	352 (+4.6)	388 (−13.9)
Δ-Zn*S*L^2	≈280 (−)[b]	322 (+0.9)	350 (−2.0)	387 (+14.9)
Λ-Zn*R*L^3	281 (+11)	322 (−1.4)	355 (+3.7)	389 (−15.5)
Δ-Zn*S*L^3	279 (−12)	321 (+1.7)	354 (−2.6)	388 (+16.2)

[a] λ in nm and Δε in L mol^{-1} cm^{-1}. [b] Noisy signal, only sign given.

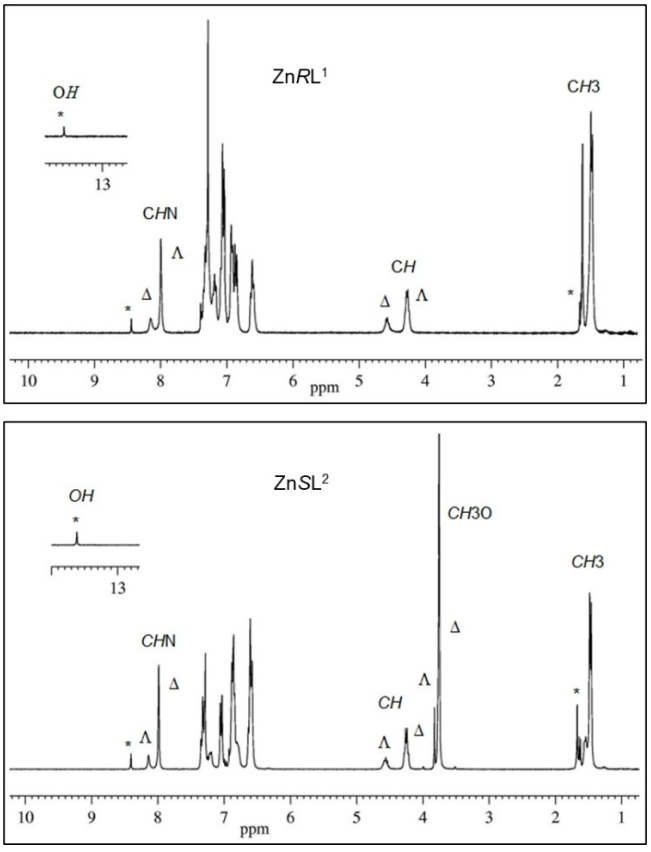

Figure 7. ^{1}H NMR spectra for Zn*R*L^1 and Zn*S*L^2 (showing Λ- and Δ-diastereomers) in $CDCl_3$ (asterisked peaks correspond to the free Schiff base ligands liberated from decomposition of the complexes upon dissolution).

at ca. δ 13.60 ppm reveals the presence of a small amount of free Schiff base ligand (< 5 %) liberated through decomposition of the complex upon dissolution in solution.

^{1}H NMR spectra in solution show two sets of peaks for each proton separated by around 0.10–0.25 ppm with an uneven ratio, corresponding to the presence of both the Λ and Δ-diastereomers in the bulk samples of the complexes.[16,17,21] The peak assignments for the Λ- or Δ-diastereomers are based on the assumption that the diastereomer found in the solid state, namely Λ-Zn*R*L$^{1-3}$ or Δ-Zn*S*L$^{1-3}$, prevails as the major diastereomer in solution immediately after dissolution. As we shall see below, this hypothesis is confirmed by NMR and ECD calculations. The major diastereomers Λ-Zn*R*L$^{1-3}$ or Δ-Zn*S*L$^{1-3}$, based on both the methine and imine proton peaks, are observed at relatively high field, while the oppositely configured minor diastereomers Δ-Zn*R*L$^{1-3}$ or Λ-Zn*S*L$^{1-3}$ are found at relatively low field (Table 4). The ratios of the two diastereomers are 77–82/23–18 (Δ/Λ) for Zn*S*L$^{1-3}$ and 76–81/24–19 (Λ/Δ) for Zn*R*L$^{1-3}$, estimated from the imine proton peak (Table 4). Similar diastereomeric ratios are also estimated from the methine proton peak (Table 4). This proportion for the diastereomers is in good agreement with the already reported Zn^{II}-(*R* or *S*)-(Ar)salicylaldiminate or analogous naphthaldiminate complexes.[17,21] On the contrary, the analogous Zn^{II}-(*R* or *S*)-dihalosalicylaldiminates show only one diastereomer Λ-Zn*R*L or Δ-Zn*S*L in the solution samples.[26]

The simulated ^{1}H NMR spectra for diastereomeric pairs Λ-Zn*R*L^2/Δ-Zn*R*L^2 or Δ-Zn*S*L^2/Λ-Zn*S*L^2, calculated at the GIAO B3LYP/6-311 + G(2d,p) level with PCM in chloroform, show the peaks for Λ-Zn*R*L^2 at relatively high field (based on the methine/imine proton peaks with δ = 4.64, 4.45/8.67, 7.50 ppm), while those for Δ-Zn*R*L^2 resonate at relatively lower field (δ = 6.00, 5.44/9.55, 8.49 ppm). Similarly, Δ-Zn*S*L^2 shows the peaks at relatively high field (methine/imine: δ = 4.64, 4.45/8.67,7.50 ppm), while those for Λ-Zn*S*L^2 appear at relatively low field (δ = 5.29, 4.72/8.83, 7.77 ppm). These results support the peak assignment for the experimental spectra for Zn*R*L$^{1-3}$ or Zn*S*L$^{1-3}$ in solution, as discussed above (Figure 7 and Table 4).

Table 4. Percentages (%) of Λ/Δ-diastereomers in Zn*R*L$^{1-3}$ or Zn*S*L$^{1-3}$ in $CDCl_3$ at 20 °C (estimated from the imine, methine and methyl proton peaks, respectively).

Entry	Imine proton [a]		Methine proton [a]		Methyl protons [a]	
	Λ [%]	Λ [%]	Λ [%]	Λ [%]	Λ [%]	Λ [%]
Λ-Zn*R*L^1	8.00 (76)	8.14 (24)	4.27 (76)	4.58 (24)	1.48[b]	1.48[b]
Δ-Zn*S*L^1	7.96 (81)	8.11 (19)	4.22 (78)	4.55 (22)	1.45 (80)	1.53 (20)
Λ-Zn*R*L^2	8.03 (80)	8.15 (20)	4.21 (82)	18 (4.54)	1.51[b]	1.51[b]
Δ-Zn*S*L^2	8.13 (23)	7.97 (77)	4.56 (27)	4.25 (73)	1.51 (23)	1.46 (77)
Λ-Zn*R*L^3	8.14 (22)	7.98 (78)	4.62 (25)	4.25 (75)	1.56 (22)	1.52 (78)
Δ-Zn*S*L^3	8.15 (18)	8.03 (82)	4.57 (18)	4.21 (82)	1.50[b]	1.50[b]

[a] δ (ppm). [b] Peaks for Λ-and Δ-diastereomers are overlapped.

Effects of Temperature and Time on the Δ⇆Λ Equilibrium

As the complexes show two separate peaks for each proton, corresponding to the Δ- and Λ-diastereomers in solution, there might be a thermodynamic equilibrium between the two diastereomers (Δ⇆Λ) which will be shifted by changing the temperature.[21,26] To check this hypothesis, ^{1}H NMR spectra for Zn*S*L^1 were run at variable temperatures starting from 20 °C to 0 °C, −20 °C and −40 °C in $CDCl_3$ (Figure 8). The spectral analyses reveal that the diastereomeric ratio (Δ:Λ) changes from 74:26 (20 °C) to 77:23 (0 °C), 80:20 (−20 °C) and 83:17 (−40 °C), respectively (Table 5). These results suggest an equilibrium between the two diastereomers which favors the most stable Δ-*S*-form at low temperature in solution, with the fraction of the less stable Λ-*S*-form increasing at higher temperatures (Figure 8). Indeed, the plot of diastereomeric ratio (Δ:Λ) vs. T (°C) shows a quasi-linear relationship, indicating the presence of a diastereomeric equilibrium (Δ⇆Λ) in solution (Figure 9). The equilibrium constant of such a process amounts to 2.8 at 293 K (20 °C), corresponding to a free energy difference $\Delta G^0 = 0.6$ kcal mol^{-1} between the two species.

^{1}H NMR spectra at different time intervals after dissolution might also show an equilibrium (Δ⇆Λ) shift provided that the equilibrium is slow enough with respect to the NMR time scale.[16,17,21,26] To check this equilibrium shift, we recorded ^{1}H NMR spectra for Zn*S*L^1 or Zn*R*L^1 in $CDCl_3$ at different time intervals after dissolution of the sample. The spectral analyses demonstrate that the diastereomeric ratios (Δ:Λ or Λ:Δ) remain almost unchanged (data not shown), suggesting no equilibrium shift in course of time in solution, in line with our previous findings for Zn-(*R* or *S*)-(Ar)naphthaldiminates.[21] On the contrary, a diastereomeric equilibrium shift as a function of complex dissolution time was reported from a single diastereomer (within 10 min) to a diastereomeric mixture of 33/67 (40 min) and 46/54 (36 h) in Zn-(*R*/*S*)-2-((2-OH-2-phenylethylimino)methyl)phenoxidates.[16]

Variable-temperature ECD spectra were measured in chloroform for compounds Zn*S*L^1 and Zn*S*L^3 between 20 and 60 °C (Figure 10). The major ECD couplet in the region between 340 and 420 nm features an intensity decrease to respectively 50 % and 40 % for Zn*S*L^1 and Zn*S*L^3 upon heating. An isodichroic point is observed in correspondence with the couplet crossover (i.e., where the ECD curve crosses the zero line) at 365 nm. This is also consistent with a diastereomeric equilibrium between two species (Λ⇆Δ) showing ECD spectra with opposite sign in

Table 5. Changes of Δ- and Λ-diastereomers (%) in Zn*S*L^1 at variable temperatures in $CDCl_3$.[a]

Temperature [°C]	Δ-diastereomer [%]	Λ-diastereomer [%]
20	74	26
0	77	23
−20	80	20
−40	83	17

[a] Values of Δ/Λ-diastereomers are estimated from the imine or methyl proton peaks.

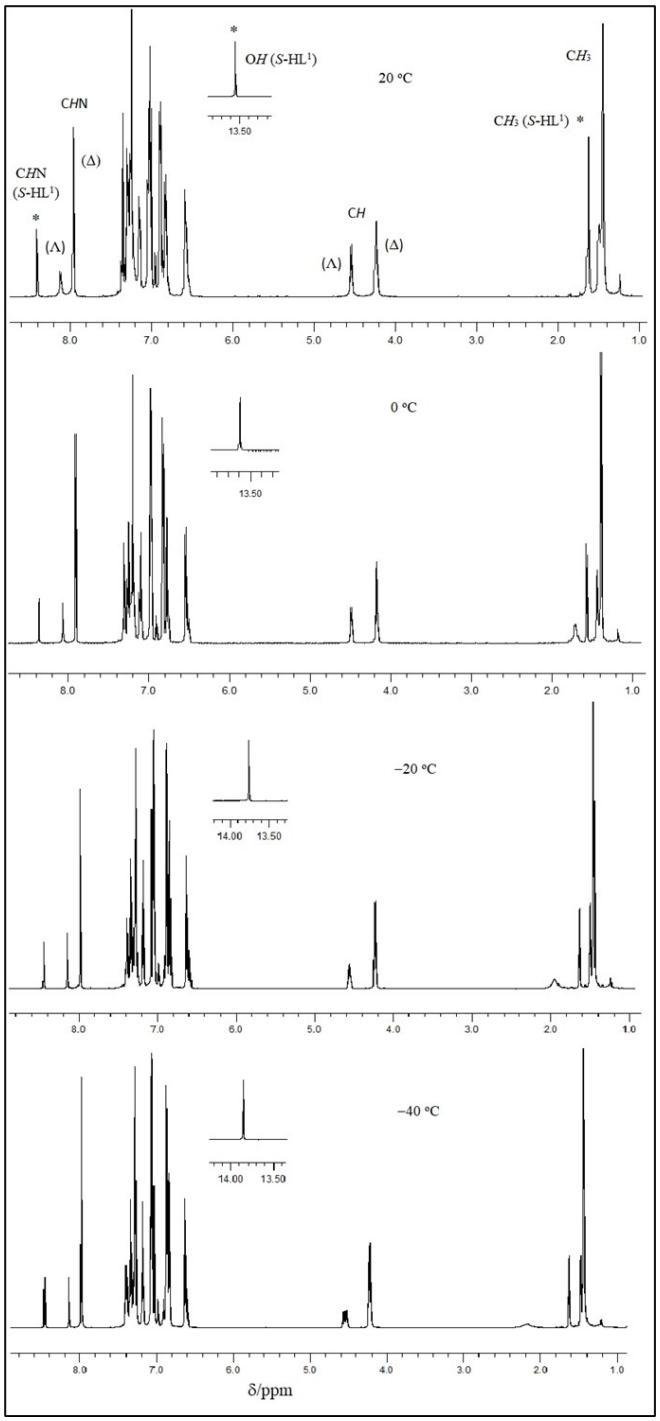

Figure 8. ^{1}H NMR spectra for Zn*SL*^{1} at different temperatures in $CDCl_3$ (asterisked peaks correspond to the free ligand (*S*-HL^1) in the samples). The *CH* peak for the free ligand overlaps with the Λ-diastereomer peak.

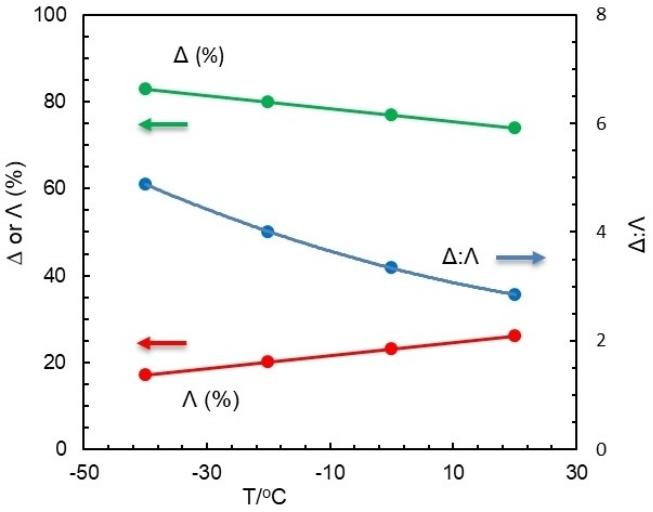

Figure 9. Plot of Δ- or Λ-diastereomer (%) and diastereomeric ratios Δ:Λ (%) vs. T (°C) for Zn*SL*^{1} in $CDCl_3$.

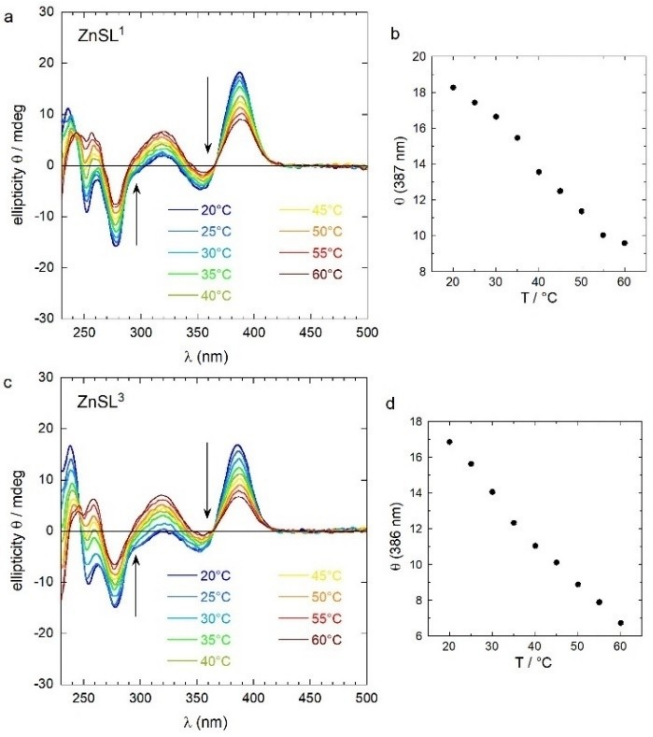

Figure 10. Variable-temperature ECD spectra for Zn*SL*^{1} (up) and Zn*SL*^{3} (bottom) 0.60 mM in chloroform, cell path length 0.5 mm. On the sides: plot of ellipticity at 386–387 nm (positive maximum) as a function of temperature.

that region, as will be confirmed by TD-DFT calculations.[21] In other regions of the spectrum, however, the effect of heating is less straightforward; for example, the band at 318.5 nm is increased in intensity. Thus, more than a single equilibrium phenomenon is responsible for the thermally induced evolution of the ECD spectra at high temperature, possibly a combination of a diastereomeric equilibrium and conformational rearrangements.

Effects of Solvent on Diastereomeric Ratio (Δ:Λ)

^{1}H NMR spectra for Zn*SL*^{2} were recorded in different solvents including acetone-d_6, CD_3OD, $CDCl_3$, CD_2Cl_2, toluene-d_8 and

DMSO-d_6 at 25 °C (Figure S6). The spectra show the presence of both Δ- and Λ-diastereomers with varying ratios in all solvents. The spectral analysis further reveals that the Δ:Λ ratio substantially changes with the polarity of the solvents from 93:7 (acetone-d_6) to 91:9 (CD_3OD), 88:12 (DMSO-d_6), 78:22 ($CDCl_3$), 74:26 (CD_2Cl_2) and finally, to 69:31 (toluene-d_8) (Table 6). Indeed, the plot of Δ or Λ fraction vs. the dielectric constant (ε_r) of the solvents suggests (Figure 11) that an increase of solvent polarity further favors the Δ-*S*-diastereomer, while a decrease favors – relatively – the Λ-diastereomer. It must be noticed, however, that the trend shown in Figure 11 is not regular; the largest Δ:Λ ratio is observed for acetone-d_6 rather than for the two more polar solvents. This means that the equilibrium cannot be simply described by the Onsager model (solvent reaction field), and specific solute-solvent interactions also come into play.[32]

Geometry Optimizations and ECD Calculations

Geometry optimizations run at the B3LYP-D3BJ/6-311G + (d,p) level with PCM for chloroform revealed a clear preference for Λ-Zn*R*L$^{1-3}$ or Δ-Zn*S*L$^{1-3}$ vs. Δ-Zn*R*L$^{1-3}$ or Λ-Zn*S*L$^{1-3}$ (Figures S7-S9) in parallel to the solid-state X-ray structures and NMR evidence. For all compounds, the calculated population of the major diastereomer was > 99%. For compound ZnL^1, a different functional (ωB97X-D/6-311G + (d,p)/PCM) led to consistent results, too. Thus, DFT calculations predict the major diastereomeric species correctly, but overestimate its relative stability when compared to NMR data. The most stable structure found for Λ-Zn*R*L^1 or Δ-Zn*S*L^1, with population > 97.5% with both functionals, is similar to the X-ray geometry: the root-mean-square deviation (RMSD) for the heavy (non-H) atoms between the two structures is 0.47 Å (Figure S10).

Table 6. Proportion of Λ- and Δ-diastereomers (%) for Zn*S*L^2 in different solvents at 25 °C (estimated from the imine proton peak).

Solvents	Λ (%) (δ ca. 8.12 ppm)	Δ (%) (δ ca. 7.95 ppm)
Acetone-d_6	7	93
CD_3OD	9	91
DMSO-d_6	12	88
$CDCl_3$	22	78
CD_2Cl_2	26	74
Toluene-d_8	31	69

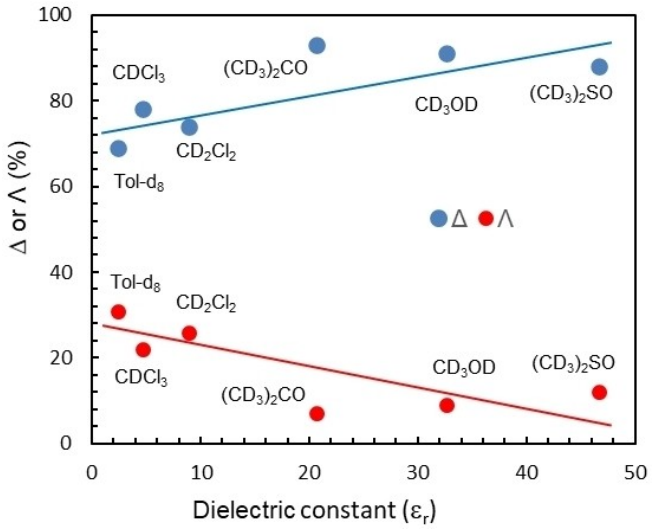

Figure 11. Plot of Δ or Λ fraction vs. dielectric constant (ε_r) of the solvents for Zn*S*L^2 at 25 °C (values are calculated from the imine proton peak).

Excited-state calculations were run with the TD-DFT method employing CAM-B3LYP and B3LYP functionals, the def2-TZVP basis set, PCM model for chloroform, and using the structures optimized at the B3LYP-D3BJ/6-311G + (d,p)/PCM level. The absorption spectra calculated for all species ZnL$^{1-3}$, as well as for the diastereomeric pair Λ/Δ-Zn*R*L$^{1-3}$, were all consistent with each other (Figure S11). To avoid ambiguity, the results for the *R*-configured ligands are discussed here; calculations for *S*-configured ligands were fully consistent. The simulated ECD spectra for the diastereomeric pairs Λ-Zn*R*L^1 and Δ-Zn*R*L^1 exhibit mirror-image relationship on a wide wavelength range (Figure 12). As the d^{10} Zn^{2+} core does not originate any allowed d−d transition, the absolute configuration of the metal center can be assessed from metal−ligand and/or *intra*-ligand transitions bands in the UV region.[21,26] In particular, complexes with Λ chirality atmetal are correlated with a first negative calculated ECD band, followed by a positive one. The opposite occurs for Δ chirality atmetal. Thus, we can establish the following relationship: a negative couplet in the region between 320 and 420 nm corresponds to Λ chirality atmetal, while a positive couplet in the same region corresponds to Δ chirality atmetal. The fact that diastereomeric structures of the kind Λ-Zn*R*L^1 vs. Δ-Zn*R*L^1 lend almost mirror-image ECD spectra signifies that they are dominated by the chirality atmetal rather than by the chirality at the carbon atoms, although it is this latter which dictate the former through diastereoselection. Similar results have been found before for different families of M^{II}-(Ar)-salicylaldiminato/naphthaldiminato complexes.[17–26] Molecular orbital analysis of the diagnostic bands confirms they are due to exciton-coupled MLCT-type transitions (Figure S12). The occupied orbitals (HOMO and HOMO − 1) are a combination of metal d orbitals (d_{xy} and d_{yz}) and ligand π orbitals, while the virtual (LUMO) orbital is a ligand π* orbital. The observed sign of the ECD couplet is in line with the expectations of exciton chirality theory, based both on qualitative arguments and a quantitative assessment (Figures S13-S14).[33] It is noteworthy that the analogous naphthaldimine Schiff base complexes exhibited an apparent exception of the exciton chirality rule for the corresponding ECD couplet in the 340–440 nm region.[21]

Comparison of experimental ECD spectra of complexes ZnL$^{1-3}$ with Boltzmann-averaged calculated spectra reveals a satisfactory agreement, using both the CAM-B3LYP (Figure 13) and the B3LYP functional (Figure S15). Recalling that the estimated diastereomeric populations (used to generate Boltzmann-averaged spectra) are dominated by Λ-Zn*R*L$^{1-3}$ and Δ-Zn*S*L$^{1-3}$ species, respectively, the results strongly suggest that the Zn*R*L$^{1-3}$ or Zn*S*L$^{1-3}$ complexes result in a diastereomeric excess of Λ-Zn*R*L$^{1-3}$ or Δ-Zn*S*L$^{1-3}$ (as major diastereomer) in

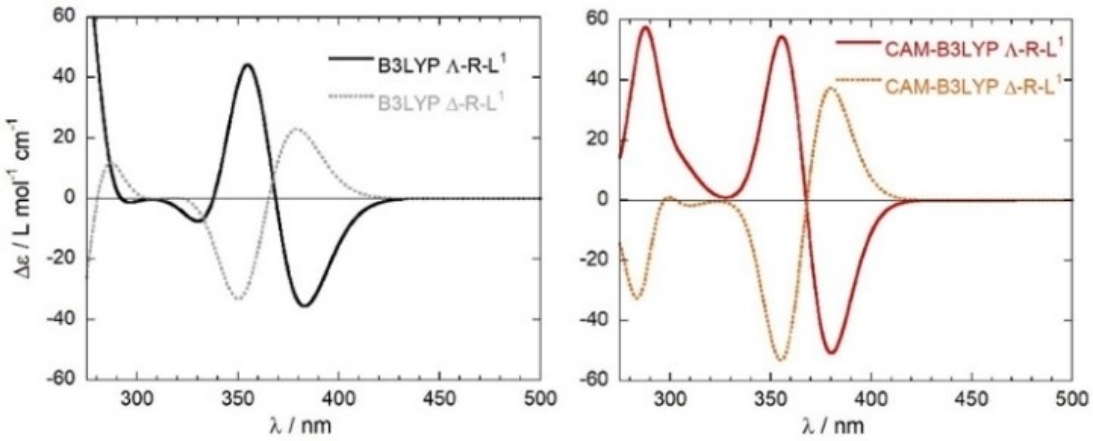

Figure 12. ECD spectra calculated for the two diastereomers Λ-Zn*R*L[1] (solid lines, average of 3 conformers) and Δ-Zn*R*L[1] (dotted lines, average of 4 conformers). Calculations were run at the B3LYP/def2-TZVP/PCM (left) and CAM–B3LYP/def2-TZVP/PCM (right) levels, using the PCM model for chloroform. Geometry optimizations were run at the B3LYP-D3BJ/6-311 + G(d,p)/PCM level. Spectra were convoluted as sums of Gaussians with exponential bandwidth σ = 0.2 eV; CAM–B3LYP spectra are red-shifted by 40 nm, and B3LYP spectra by 5 nm.

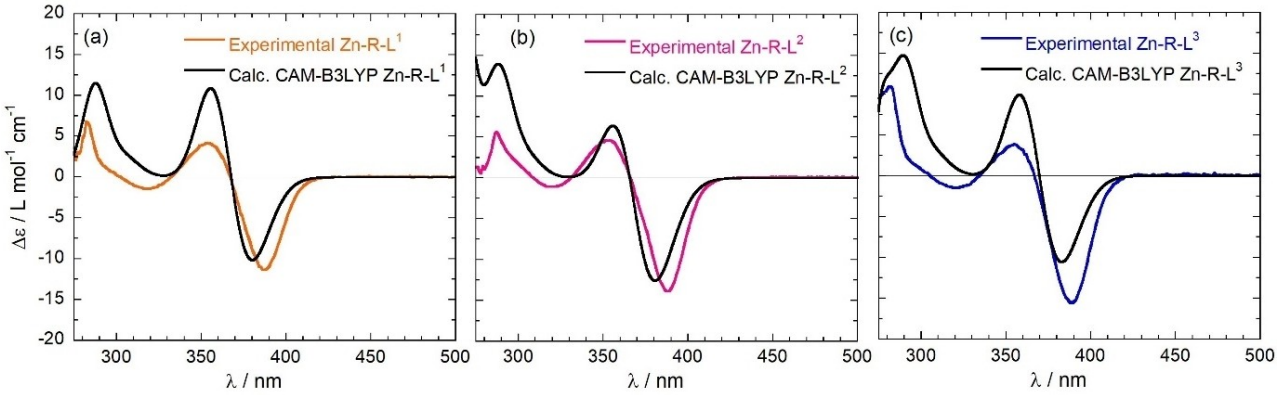

Figure 13. Comparison between experimental and calculated ECD spectra for (a) Zn*R*L[1], (b) Zn*R*L[2] and (c) Zn*R*L[3]. Calculations run at the CAM–B3LYP/def2-TZVP/PCM//B3LYP-D3BJ/6-311 + G(d,p)/PCM level with a PCM level for chloroform. Calculated spectra were convoluted as sums of Gaussians with exponential bandwidth σ = 0.2 eV, red-shifted by 5–7 nm, and scaled by a factor 5 (a and c) or 3 (b).

solution. This result is in line with the X-ray structures for Λ-Zn*R*L[1−3] or Δ-Zn*S*[1−3] in solid state,[5c–d,17,21,26] ^{1}H NMR evidence, VT-ECD results, and DFT optimization findings discussed above.

Overall, we observe a conservation of Λ or Δ-chirality-at-metal induction in the *R* or *S*-ligated complexes (i.e., Λ-M*R*L or Δ-M*S*L) resulting from diastereoselection in solid and solution phases (or gas-phase optimized structures), as observed for a series of analogues M^{II}-(*R* or *S*)-(Ar)salicylaldiminates/naphthaldiminates (M=Co,[22,25] Ni,[20] Cu,[18,19] and Zn[5c–d,17,21,26]). In contrast, solid-versus-solution studies reveal solvation-induced chirality-at-metal inversion in Cu^{II}-(*R*)-(*p*-CH_3O)salicylaldiminates[19] and Cu^{II}-(*R* or *S*)-1-*N*-(phenyl)-2,4-dihalogen-salicylaldiminates.[23]

Conclusion

We have reported the synthesis and thorough investigation of a family of bis[(*R* or *S*)-*N*-1-(Ar)ethylsalicylaldiminato-κ^{2}N,O]-Δ/Λ-zinc(II) {Ar=C_6H_5 (Zn*R*L[1] or Zn*S*L[1]), *p*-$CH_3OC_6H_4$ (Zn*R*L[2] or Zn*S*L[2]) and *p*-ClC_6H_4 (Zn*R*L[3] or Zn*S*L[3])} compounds. This series allowed us to complete our survey on the homoleptic series of ligands HL[1]-HL[3],[17,19,20a,22] and provided new comparison with the analogous Zn^{II}-(Ar)naphthaldiminate series.[21] The solid-state properties were characterized by X-ray crystallography and powder X-ray diffraction, and solid-to-liquid phase transitions by DSC. In the solid state, a single diastereomer exists for each compound, that is, Δ-Zn*S*L or Λ-Zn*R*L. An equilibrium phenomenon was detected in solution between the diastereomeric species with opposite chirality at the metal. The equilibrium is shifted towards the species with Δ-Zn*S*L or Λ-Zn*R*L configuration in a temperature- and solvent-dependent manner. The phenomenon was evidenced and characterized by NMR and ECD spectroscopy. DFT geometry optimizations and TD-DFT calculations ultimately allowed the assignment of the chirality at-metal. It is noteworthy that the same equilibrium phenomenon, biased toward the same diastereomeric species, has been consistently found for the Schiff base complexes of several metals (Co, Zn, Ni, and Cu) with different coordination geo-

metries, and for two distinct families (salicylaldiminates and naphthaldiminates) of ligands.

Experimental Section

IR-spectra were recorded on a Nicolet iS10 spectrometer as KBr disc at ambient temperature. UV-Vis spectra were obtained with Shimadzu UV 3150 spectrophotometer in $CHCl_3$ at 25 °C. ECD spectra were obtained with OLIS RSM spectropolarimeter, Rapid Scanning Monochromator (On-line Instrument System, Inc.) in $CHCl_3$ at 20 °C. VT-ECD spectra were obtained with a Jasco J-1500 spectropolarimeter equipped with a Peltier stage. ^{1}H NMR spectra were recorded on a JEOL AC 600 spectrometer operating at 600 MHz in $CDCl_3$ at 20 °C. ^{1}H NMR spectra for Zn*S*L^2 were recorded on a Bruker Ascend 400 spectrometer operating at 400 MHz in different solvents (acetone-d_6, CD_3OD, $CDCl_3$, CD_2Cl_2, toluene-d_8 and DMSO-d_6) at 25 °C. Variable temperature ^{1}H NMR spectra for Zn*S*L^1 were recorded on a Bruker Ascend 400 spectrometer operating at 400 MHz in $CDCl_3$ at 25 °C. Electron impact (EI) mass spectra were recorded with a Thermo-Finnigan TSQ 700. Isotopic distribution patterns for the Zn or Zn + Cl containing ions are clearly visible in the spectra and the peaks arising from the most abundant ^{64}Zn/^{35}Cl isotopes are listed. Differential Scanning Calorimetery (DSC) were run on a Shimadzu DSC-60 in the range 20-200 °C (just before any decomposition temperature) with a rate of 10 K min^{-1} under nitrogen atmosphere. PXRD data were collected on a GNR Explorer Powder X-ray diffractometer operating in the Bragg–Brentano geometry with CuK_α radiation ($\lambda = 1.5406$ Å). The experiment was carried out at 40 kV and 30 mA using a silicon zero-background sample holder. Data were collected at 25 °C with 2θ step size 0.02° and an integration time of 3.0 s over an angular range of 5–50° (2θ). The enantiopure Schiff base ligands (*R* or *S*)-*N*-1-(Ar)ethylsalicylaldimine (*R* or *S*-HL$^{1-3}$) were synthesized following our previous literature.[15]

Bis{(*R*)-*N*-1-(C_6H_5)ethylsalicylaldiminato-κ^{2}N,O}-Λ/Δ-zinc(II) (Λ/Δ-Zn*R*L^1): yield 255 mg (74% based on (*R*)-*N*-1-(C_6H_5)-ethylsalicylaldimine). See Supporting Information for the compound's spectral data.

Bis{(*S*)-*N*-1-(C_6H_5)ethylsalicylaldiminato-κ^{2}N,O}-Δ/Λ-zinc(II) (Δ/Λ-Zn*S*L^1): yield 262 mg (76%).

Bis{(*R*)-*N*-1-(*p*-$CH_3OC_6H_4$)ethylsalicylaldiminato-κ^{2}N,O}-Λ/Δ-zinc(II) (Λ/Δ-Zn*R*L^2): yield 288 mg (75%).

Bis{(*S*)-*N*-1-(*p*-$CH_3OC_6H_4$)ethylsalicylaldiminato-κ^{2}N,O}-Δ/Λ-zinc(II) (Δ/Λ-Zn*S*L^2): yield 285 mg (74%).

Bis{(*R*)-*N*-1-(*p*-ClC_6H_4)ethylsalicylaldiminato-κ^{2}N,O}-Λ/Δ-zinc(II) (Λ/Δ-Zn*R*L^3): yield 275 mg (70%).

Bis{(*S*)-*N*-1-(*p*-ClC_6H_4)ethylsalicylaldiminato-κ^{2}N,O}-Δ/Λ-zinc(II) (Δ/Λ-Zn*S*L^3): yield 280 mg (72%).

Computational Section. Conformational searches and preliminary geometry optimizations were run with Spartan'20 (Wavefunction, Inc. Irvine, CA). Final optimizations and excited-state calculations were run with Gaussian 16.[34] The computational procedure employed was similar to that previously reported for several analogs.[18–26] Starting from the X-ray structure of Zn*R*L^1, the geometries for all three pairs of complexes Λ-Zn*R*L$^{1-3}$/Δ-Zn*R*L$^{1-3}$ were constructed. Conformational searches were run by varying all possible rotatable bonds and keeping O–Zn and N–Zn distances fixed. All structures thus obtained were pre-optimized at B3LYP-D3/6-31G(d) level in vacuo, then fully optimized at B3LYP-D3BJ/6-311G + (d,p) level including PCM solvent model for chloroform. The most stable structures are shown in Figures S7-S9. Excited state properties (UV-Vis and ECD spectra) were calculated with two different functionals (B3LYP and CAM-BLYP), the def2-TZVP basis set, and PCM solvent model for chloroform. For each calculation, 36 excited states (roots) were included. The computed spectra (UV-Vis/ECD) were generated with SpecDis[35] assuming a Gaussian band shape with exponential half-width $\sigma = 0.2$ eV. ^{1}H NMR spectra were computed at GIAO B3LYP/6-311 + G(2d,p) with PCM in chloroform for diastereomeric pairs Δ/Λ-Zn*S*L^2 and Λ/Δ-Zn*R*L^2 based on the optimized structures at B3LYP/6-31G(d) level. Assessments of Δ- and Λ-diastereomers were done following these computed spectra and found in good accord to the experimental results.

X-Ray Crystallography. Structure for compound Λ-Zn*R*L^1 is a re-determination of the structure described in H. Sakiyama, H. Okawa, N. Matsumoto, S. Kida, *J. Chem. Soc., Dalton Trans.* **1990**, 2935–2939.[5c] The 'Sakiyama' structure has been deposited as CCDC 1185213. We note that in this deposited 'Sakiyama' structure, H atoms are missing on the aromatic and imine C=N carbon atoms C7, C22, C27, C32, C37 and C52. At the same time there are two instead of one H atom on the aromatic carbon atoms C2 and C26. Single crystals of Λ-Zn*R*L^1 were carefully selected under a polarizing microscope and mounted on a loop. *Data collection*: Bruker APEX II CCD diffractometer with graphite- or multi-layer mirror monochromated Mo-K_α radiation ($\lambda = 0.71073$ Å); ω-scans. Data collection and cell refinement with APEX2[36] data reduction with SAINT (Bruker).[37] *Structure analysis and refinement:* The structures were solved by direct methods (SHELXT-2015),[37] refinement was done by full-matrix least squares on F^2 using the SHELXL-2017/1 program suite, empirical (multi-scan) absorption correction with SADABS (Bruker).[38,39] All non-hydrogen positions were refined with anisotropic temperature factors. Hydrogen atoms for aromatic and olefinic CH, aliphatic CH and CH_3 groups were positioned geometrically (C–H = 0.94 Å for aromatic and olefinic CH, 0.99 for aliphatic CH and 0.97 Å for CH_3,) and refined using a riding model (AFIX 43 for aromatic/olefinic CH, AFIX 13 for aliphatic CH, AFIX 137 for CH_3), with $U_{iso}(H) = 1.2\ U_{eq}(CH)$ and $U_{iso}(H) = 1.5\ U_{eq}(CH_3)$. Details of the X-ray structure determinations and refinements are provided in Table S2. Graphics were drawn with DIAMOND (Version 4.4). Deposition Number href=https://www.ccdc.cam.ac.uk/services/structures?id=doi:10.1002/open.202200116 2157176 (for Λ-Zn*R*L^1) contains the supplementary crystallographic data for this paper. These data are provided free of charge by the joint Cambridge Crystallographic Data Centre and Fachinformationszentrum Karlsruhe href=http://www.ccdc.cam.ac.uk/structures Access Structures service.

Acknowledgements

We acknowledge the Wazed Miah Science Research Centre (WMSRC) at Jahangirnagar University, Dhaka, Bangladesh for obtaining elemental analyses and PXRD data. The authors are grateful to Alexander von Humboldt Foundation (AvH), Bonn, Germany for financial support under the project Research Group Linkage Program. We thank Prof. Andrew Woolley, Department of Chemistry, University of Toronto, Canada, for running ECD spectra. G. P. gratefully acknowledges University of Pisa for the availability of high-performance computing resources and support through the service computing@unipi, and the CINECA award under the ISCRA initiative for the availability of high-performance computing resources and support.

Conflict of Interest

The authors declare no conflict of interest.

Data Availability Statement

The data that support the findings of this study are available in the supplementary material of this article.

Keywords: chirality · diastereomeric equilibrium · metal complexes · Schiff base ligand · spectroscopic investigation

[1] a) K. R. Jain, W. A. Herrmann, F. E. Kühn, *Coord. Chem. Rev.* **2008**, *252*, 556; b) Z.-X. Xu, Z.-T. Huang, C.-F. Chen, *Tetrahedron Lett.* **2009**, *50*, 5430; c) J. Niemeyer, G. Kehr, R. Frohlich, G. Erker, *Dalton Trans.* **2009**, 3731; d) P. Adão, J. Costa Pessoa, R. T. Henriques, M. L. Kuznetsov, F. Avecilla, M. R. Maurya, U. Kumar, I. Correia, *Inorg. Chem.* **2009**, *48*, 3542; e) E. C. Escudero-Adán, M. M. Belmonte, J. Benet-Buchholz, A. W. Kleij, *Org. Lett.* **2010**, *12*, 4592; f) W. Clegg, R. W. Harrington, M. North, R. Pasquale, *Chem. Eur. J.* **2010**, *16*, 6828; g) J.-J. Lee, F.-Z. Yang, Y.-F. Lin, Y.-C. Chang, K.-H. Yu, M.-C. Chang, G.-H. Lee, Y.-H. Liu, Y. Wang, S.-T. Liu, J.-T. Chen, *Dalton Trans.* **2008**, 5945; h) M. Shibasaki, M. Kanai, S. Matsunaga, N. Kumagai, *Acc. Chem. Res.* **2009**, *42*, 1117.

[2] a) T. Hauck, K. Sünkel, W. Beck, *Z. Anorg. Allg. Chem.* **2006**, *632*, 2305; b) G. Müller, J. Brand, *Z. Anorg. Allg. Chem.* **2005**, *631*, 2820; c) H. Brunner, C. Keck, *Z. Anorg. Allg. Chem.* **2005**, *631*, 2555; d) T. J. Colacot, N. S. Hosmane, *Z. Anorg. Allg. Chem.* **2005**, *631*, 2659; e) R. Urban, D. Veghini, H. Berke, W. Beck, *Z. Anorg. Allg. Chem.* **2005**, *631*, 2715; f) P. G. Cozzi, *Chem. Soc. Rev.* **2004**, *33*, 410; g) G. M. Sammis, E. N. Jacobsen, *J. Am. Chem. Soc.* **2003**, *125*, 4442; h) R. Dreos, G. Nardin, L. Randaccio, P. Siega, G. Tauzher, *Inorg. Chem.* **2004**, *43*, 3433.

[3] a) R. Urban, W Beck, *Z. Naturforsch. B: J. Chem. Sci.* **2005**, *60*, 1071; b) B. Paul, C. Nather, K. M. Fromm, C. Janiak, *CrystEngComm.* **2005**, *7*, 309; c) W. Hoffmueller, H. Dialer, W. Beck, *Z. Naturforsch. B: J. Chem. Sci.* **2005**, *60*, 1278; d) M. J. Plater, T. Gelbrich, M. B. Hursthouse, B. M. D. Silva, *CrystEngComm.* **2006**, *8*, 895; e) S. George, S. Lipstman, S. Muniappan, I. Goldberg, *CrystEngComm.* **2006**, *8*, 417; f) X. Zhou, J. Zhao, A. M. Santos, F. E. Kuehn, *Z. Naturforsch. B: Chem. Sci.* **2004**, *59*, 1223.

[4] a) H. Brunner, H. Leyerer, *J. Organomet. Chem.* **1987**, *334*, 369; b) H. Brunner, H. Fisch, *J. Organomet. Chem.* **1987**, *335*, 1; c) B. Wisser, Y. Lu, C. Janiak, *Z. Anorg. Allg. Chem.* **2007**, *633*, 1189; d) B. Wisser, C. Janiak, *Z. Anorg. Allg. Chem.* **2007**, *633*, 1796; e) S. Klingelhöfer, M. Wiebcke, P. Behrens, *Z. Anorg. Allg. Chem.* **2007**, *633*, 113; f) T. Ederer, R. S. Herrick, W Beck, *Z. Anorg. Allg. Chem.* **2007**, *633*, 235.

[5] a) C. Evans, D. Luneau, *J. Chem. Soc. Dalton Trans.* **2002**, 83; b) H. Sakiyama, H. Okawa, N. Matsumoto, S. Kida, *Bull. Chem. Soc. Jpn.* **1991**, *64*, 2644; c) H. Sakiyama, H. Okawa, N. Matsumoto, S. Kida, *J. Chem. Soc. Dalton Trans.* **1990**, 2935; d) M. F. Pastor, T. J. J. Whitehorne, P. O. Oguadinma, F. Schaper, *Inorg. Chem. Commun.* **2011**, *14*, 1737; e) H. Ōkawa, M. Nakamura, S. Kida, *Inorg. Chim. Acta* **1986**, *120*, 185.

[6] a) R. Fleischer, H. Wunderlich, M. Braun, *Eur. J. Org. Chem.* **1998**, 1063; b) C. P. Pradeep, P. S. Zacharias, S. K. Das, *Inorg. Chem. Commun.* **2008**, *11*, 89; c) C. P. Pradeep, P. S. Zacharias, S. K. Das, *Eur. J. Inorg. Chem.* **2007**, 5377; d) C. P. Pradeep, P. S. Zacharias, S. K. Das, *Eur. J. Inorg. Chem.* **2005**, 3405; e) C. P. Pradeep, S. K. Das, *Polyhedron* **2009**, *28*, 630.

[7] a) G.-P. Li, Q.-C. Yang, Y.-Q. Tang, Y.-D. Guan, Z.-H. Shang, *Acta Chim. Sin. (Engl. Ed.)* **1987**, *45*, 421; b) T. Akitsu, Y. Einaga, *Polyhedron* **2006**, *25*, 1089; c) T. Akitsu, Y. Einaga, *Polyhedron* **2005**, *24*, 2933; d) T. Akitsu, Y. Einaga, *Polyhedron* **2005**, *24*, 1869; e) T. Akitsu, Y. Einaga, *Acta Crystallogr. Sect. C* **2004**, *60*, m640; f) T. Akitsu, *Polyhedron* **2007**, *26*, 2527.

[8] a) H. Brunner, T. Zwack, M. Zabel, W. Beck, A. Böhm, *Organometallics* **2003**, *22*, 1741; b) H. Brunner, R. Oeschey, B. Nuber, *J. Chem. Soc. Dalton Trans.* **1996**, 1499; c) S. K. Mandal, A. R. Chakravarty, *J. Chem. Soc. Dalton Trans.* **1992**, 1627; d) S. K. Mandal, A. R. Chakravarty, *J. Organomet. Chem.* **1991**, *417*, C59.

[9] a) M. Itagaki, K. Hagiya, M. Kamitamari, K. Masumoto, K. Suenobu, Y. Yamamoto, *Tetrahedron* **2004**, *60*, 7835; b) Z. Li, G. Liu, Z. Zheng, H. Chen, *Tetrahedron* **2000**, *56*, 7187; c) S. P. Rath, T. Ghosh, S. Mondal, *Polyhedron* **1997**, *16*, 4179; d) C. Gan, G. Lai, Z. Zhang, Z. Wang, M.-M. Zhou, *Tetrahedron: Asymmetry* **2006**, *17*, 725.

[10] a) R. D. Chakravarthy, K. Suresh, V. Ramkumar, D. K. Chand, *Inorg. Chim. Acta* **2011**, *376*, 57; b) C. Zhang, G. Rheinwald, V. Lozan, B. Wu, P.-G. Lassahn, H. Lang, C. Janiak, *Z. Anorg. Allg. Chem.* **2002**, *628*, 1259; c) L. Z. Flores-Lopéz, M. Parra-Hake, R. Somanathan, P. J. Walsh, *Organometallics* **2000**, *19*, 2153; d) H. Brunner, M. Niemetz, M. Zabel, *Z. Naturforsch. B: J. Chem. Sci.* **2000**, *55*, 145.

[11] a) A. Zulauf, M. Mellah, X. Hong, E. Schulz, *Dalton Trans.* **2010**, *39*, 6911; b) L.-L. Lin, X.-H. Liu, X.-M. Feng, *Progr. Chem.* **2010**, *22*, 1353; c) K. C. Gupta, A. K. Sutar, C.-C. Lin, *Coord. Chem. Rev.* **2009**, *253*, 1926; d) S. H. R. Abdi, R. I. Kureshy, N. H. Khan, V. J. Mayani, H. C. Bajaj, *Catal. Surv. Asia* **2009**, *13*, 104.

[12] a) K. Matsumoto, B. Saito, T. Katsuki, *Chem. Commun.* **2007**, 3619; b) K. C. Gupta, A. K. Sutar, *Coord. Chem. Rev.* **2008**, *252*, 1420; c) Z. Chu, W. Huang, L. Wang, S. Gou, *Polyhedron* **2008**, *27*, 1079; d) G. M. Sammis, H. Danjo, E. N. Jacobsen, *J. Am. Chem. Soc.* **2004**, *126*, 9928; e) J. F. Larrow, E. N. Jacobsen, *Top. Organomet. Chem.* **2004**, *6*, 123.

[13] a) D. Koch, W. Hoffmuller, K. Polborn, W. Beck, *Z. Naturforsch. B: Chem. Sci.* **2001**, *56*, 403; b) I. Karamé, M. Jahjah, A. Messaoudi, M. L. Tommasino, M. Lemaire, *Tetrahedron: Asymmetry* **2004**, *15*, 1569; c) I. Karamé, M. L. Tommasino, R. Faure, M. Lemaire, *Eur. J. Org. Chem.* **2003**, 1271.

[14] a) Z.-H. Yang, L.-X. Wang, Z.-H. Zhou, Q.-L. Zhou, C.-C. Tang, *Tetrahedron: Asymmetry* **2001**, *12*, 1579; b) P. Guo, K.-Y. Wong, *Electrochem. Commun.* **1999**, *1*, 559; c) E. D. McKenzie, S. J. Selvey, *Inorg. Chim. Acta* **1985**, *101*, 127; d) A. L. Iglesias, G. Aguirre, R. Somanathan, M. Parra-Hake, *Polyhedron* **2004**, *23*, 3051.

[15] a) M. Enamullah, A. Uddin, A. C. Chamayou, C. Janiak, *Z. Naturforsch., B: J. Chem. Sci.* **2007**, *62*, 807; b) M. Enamullah, A. R. Uddin, G. Hogarth, C. Janiak, *Inorg. Chim. Acta* **2012**, *387*, 173.

[16] M. Enamullah, V. Vasylyeva, C. Janiak, *Inorg. Chim. Acta* **2013**, *408*, 109.

[17] A.-C. Chamayou, S. Lüdeke, V. Brecht, T. B. Freedman, L. A. Nafie, C. Janiak, *Inorg. Chem.* **2011**, *50*, 11363.

[18] M. Enamullah, A. K. M. Royhan Uddin, G. Pescitelli, R. Berardozzi, G. Makhloufi, V. Vasylyeva, A.-C. Chamayou, C. Janiak, *Dalton Trans.* **2014**, *43*, 3313.

[19] A.-C. Chamayou, G. Makhloufi, L. A. Nafie, C. Janiak, S. Lüdeke, *Inorg. Chem.* **2015**, *54*, 2193.

[20] a) M. Enamullah, M. A. Quddus, M. R. Hasan, G. Pescitelli, R. Berardozzi, G. J. Reiß, C. Janiak, *Eur. J. Inorg. Chem.* **2015**, 2758; b) M. Enamullah, M. A. Quddus, M. R. Hasan, G. Pescitelli, R. Berardozzi, G. Makhloufi, V. Vasylyeva, C. Janiak, *Dalton Trans.* **2016**, *45*, 667.

[21] M. Enamullah, G. Makhloufi, R. Ahmed, B. Alif Joy, M. A. Islam, D. Padula, H. Hunter, G. Pescitelli, C. Janiak, *Inorg. Chem.* **2016**, *55*, 6449.

[22] G. Pescitelli, S. Lüdeke, A.-C. Chamayou, M. Marolt, V. Justus, M. Górecki, L. Arrico, L. Di Bari, M. A. Islam, I. Gruber, M. Enamullah, C. Janiak, *Inorg. Chem.* **2018**, *57*, 13397.

[23] N. Kordestani, H. A. Rudbari, G. Bruno, S. Rosario, J. D. Braun, D. E. Herbert, O. Blacque, I. Correia, M. A1-M. Zaman, M. M. Bindu, C. Janiak, M. Enamullah, *Dalton Trans.* **2020**, *49*, 8247.

[24] M. Enamullah, M. Anwar, M. K. Islam, D. Woschko, C. Janiak, *Dalton Trans.* **2021**, *50*, 9236.

[25] M. Górecki, M. Enamullah, M. A. Islam, M. K. Islam, S.-P Höfert, D. Woschko, C. Janiak, G. Pescitelli, *Inorg. Chem.* **2021**, *60*, 14116.

[26] H. A. Rudbari, A. Saadati, M. Aryaeifar, O. Blacque, I. Correia, M. K. Islam, C. Janiak, M. Enamullah, *Dalton Trans.* **2022**, *51*, 2385.

[27] a) A. Damas, J. Moussa, M. N. Rager, H. Amouri, *Chirality* **2010**, 22, 889; b) L. Mimassi, C. Guyard-Duhayon, M. N. Rager, H. Amouri, *Inorg. Chem.* **2004**, *43*, 6644; c) L. Mimassi, C. Cordier, C. Guyard-Duhayon, B. E. Mann, H. Amouri, *Organometallics* **2007**, *26*, 860.

[28] a) S. E. Howson, L. E. Allan, N. P. Chmel, G. J. Clarkson, R. van Gorkum, P. Scott, *Chem. Commun.* **2009**, 1727; b) H. Amouri, M. Gruselle, *Chirality in transition metal chemistry: Molecules, supramolecular assemblies, materials*, John Wiley & Sons, Ltd. **2008**; c) A. von Zelewsky, O. Mamula, *J. Chem. Soc. Dalton Trans.* **2000**, 219; d) A. von Zelewsky, *Stereochemistry of Coordination Compounds*, John Wiley & Sons, Chichester **1996**; e) J. M. Becker, J. Barker, G. J. Clarkson, R. van Gorkum, G. K. Johal, R. I. Walton, P. Scott, *Dalton Trans.* **2010**, *39*, 2309; f) U. Knof, A. von Zelewsky, *Angew. Chem. Int. Ed.* **1999**, *38*, 302; g) M. Seitz, S. Stempfhuber, M. Zabel, M. Schütz, O. Reiser, *Angew. Chem. Int. Ed.* **2005**, *44*, 242.

[29] a) C. Merten, R. McDonald, Y. Xu, *Inorg. Chem.* **2014**, *53*, 3177; b) M. Albrecht, E. Isaak, M. Baumert, V. Gossen, G. Raabe, R. Fröhlich, *Angew. Chem. Int. Ed.* **2011**, *50*, 2850.
[30] a) C. M. Álvarez, R. Carrillo, R. García-Rodríguez, D. Miguel, *Chem. Commun.* **2011**, *47*, 12765; b) J. Gregoliński, M. Hikita, T. Sakamoto, H. Sugimoto, H. Tsukube, H. Miyake, *Inorg. Chem.* **2016**, *55*, 633; c) S. Zahn, J. W. Canary, *Science* **2000**, *288*, 1404.
[31] T. Onodera, T. Akitsu, *Polyhedron* **2013**, *59*, 107.
[32] M. Pollastrini, F. Lipparini, L. Pasquinelli, F. Balzano, G. U. Barretta, G. Pescitelli, G. Angelici, *J. Org. Chem.* **2021**, *86*, 7946.
[33] G. Pescitelli, *Chirality* **2022**, *34*, 333.
[34] Gaussian 16, Revision C.01, M. J. Frisch, G. W. Trucks, H. B. Schlegel, G. E. Scuseria, M. A. Robb, J. R. Cheeseman, G. Scalmani, V. Barone, G. A. Petersson, H. Nakatsuji, X. Li, M. Caricato, A. V. Marenich, J. Bloino, B. G. Janesko, R. Gomperts, B. Mennucci, H. P. Hratchian, J. V. Ortiz, A. F. Izmaylov, J. L. Sonnemberg, D. Williams-Young, F. Ding, F. LIpparini, F. Egidi, J. Goings, B. Peng, A. Petrone, T. Henderson, D. Ranasinghe, V. G. Zakrzewski, J. Gao, N. Rega, G. Zheng, W. Liang, M. Hada, M. Ehara, K. Toyota, R. Fukuda, J. Hasegawa, M. Ishida, T. Nakajima, Y. Honda, O. Kitao, H. Nakai, T. Vreven, K. Throssell, J. Montgomery, J. A., J. E. Peralta, F. Ogliaro, M. Bearpark, J. J. Heyd, E. Brothers, K. N. Kudin, V. N. Staroverov, T. A. Keith, R. Kobayashi, J. Normand, K. Raghavachari, A. Rendell, J. C. Burant, S. S. Iyengar, J. Tomasi, M. Cossi, J. M. Millam, M. Klene, C. Adamo, R. Cammi, J. W. Ochterski, R. L. Martin, K. Morokuma, O. Farkas, J. B. Foresman, D. J. Fox, Gaussian, Inc., Wallingford CT **2016**.
[35] a) T. Bruhn, A. Schaumlöffel, Y. Hemberger, G. Bringmann, *Chirality* **2013**, *25*, 243; b) SpecDis, Version 1.71, T. Bruhn, A. Schaumlöffel, Y. Hemberger, G. Pescitelli, Berlin, Germany **2017**, https:/specdis-software.jimdo.com.
[36] *APEX2, Data collection program for the CCD area-detector system, Version 2.1-0*, Bruker Analytical X-ray Systems: Madison WI), **1997–2014**.
[37] *SAINT, Data reduction, frame integration program for the CCD area-detector system*, Bruker Analytical X-ray Systems: Madison WI), **1997–2014**.
[38] G. M. Sheldrick, *Program SADABS*, University of Göttingen: Göttingen, Germany **1996**.
[39] a) L. Krause, R. Herbst-Irmer, G. M. Sheldrick, D. Stalke, *J. Appl. Crystallogr.* **2015**, *48*, 3; b) K. Brandenburg, *Diamond Version 4.4), Crystal, Molecular Structure Visualization*, Crystal Impact-K. Brandenburg & H. Putz Gbr: Bonn, Germany **2017**.

Manuscript received: May 18, 2022
Revised manuscript received: May 24, 2022